Hybrid Refractive–Diffractive Optical Vortex Microlens

Zhen-Nan Tian, Xiao-Wen Cao, Wen-Gang Yao, Pei-Xin Li, Yan-Hao Yu, Gen Li, Qi-Dai Chen, and Hong-Bo Sun, *Member, IEEE*

***Abstract*— We report a novel hybrid refractive–diffractive microlens combined with spiral phase for the generation of optical vortex, which is fabricated via femtosecond laser direct writing technology. The unique optical performance of focusing capability is demonstrated. At the focus position, the hollow focus with different integer topological charges is investigated. Moreover, experimental results are supported by finite-element calculation. The novel microlens generating an optical vortex will fulfill important applications in optical manipulation, multistate information encoding, quantum communication, and computation, particularly in the compaction, integration, and simplification of optical vortex generation system.**

***Index Terms*— Femtosecond laser, hybrid refractive-diffractive, optical vortex, microlens.**

I. Introduction

LIGHT beams with a helical phase front which possess an orbital angular momentum (OAM) along their direction of propagation, can induce optical vortex (OV) as focused [1], [2]. As a novel optical phenomenon, OV beams hold the promise in various physical mechanical [3], [4], and technological applications, such as optical manipulation [5], [6], optical communication [7], quantum information, and astronomy [8], [9]. Over the past decades, efforts have been made to fabricate and design OV beams, including the geometric method [10], hologram fork dislocation grating [11], [12], spiral phase plate [13], [14], hollow optical fiber [15], [16], and changing optical parametric oscillator [17].

The above-mentioned methods are typical approaches to obtain OV beams and greatly broaden their applications. K. T. Gahagan and G. A. Swartzlander have demonstrated threedimensional radiation pressure trapping spherical particle in water using an OV beams twenty years ago [18]. Yuan et al. have recently achieved total data capacities on the order of sub-Pbit s^{-1} ($\sim 10^{14}$ bit s^{-1}) in high-speed optical communications by designing Dammann OV grating [19]. Scherer et al. have demonstrated that the OAM of photons in the OV beams can induce rotation of single silver nanowires with an overall length of 10 mm that lie on a dielectric surface [6]. The wide variety of applications propose a higher requirement for OV beams generator. However, these methods may be bulky, strongly dependent on incident light and low-integration, which restricts their better utilization in integrated optics. Specifically, the geometric method depends on the original parameters of the incident light, the methods based on the diffraction theory show limits with low diffraction efficiency and twin images, the spiral phase plate requires converging beam or an additional focus element, while the adjustment of the laser parameters is cumbersome. As a promising solution to above dilemmas, femtosecond laser direct writing (FsLDW) is a simple and rapid-writing approach with the arbitrary designability, and reasonably high spatial resolution [20]–[23].

Here, we propose a miniature and simple OV beams generator, called hybrid refractive-diffractive optical vortex microlens (HOVML). The HOVML integrates spiral phase plate on the surface of a normal microlens using femtosecond laser direct writing (FsLDW). The unique optical performance has also been simulated in far field and show consistent results with the experiments. Compared to the existing methods, our highly integrated HOVML can produce OV beams with only a single hybrid refractive-diffractive microlens. Furthermore, on account to the continuous surface structures, it possesses higher theoretical transformation efficiency than multi-levels and amplitude type diffractive element.

II. Experiments

The OAM of photons was first demonstrated by Allen *et al.* [2]. The angular momentum is associated with the spatial distribution of the electromagnetic field. An OV beam is a typical optical field with OAM, which has helical mode $\psi_{\lambda,l}\left(\vec{r}\right)$,

$$\psi_{\lambda,l}\left(\vec{r}\right) = u(r,z)e^{-ikz}e^{il\theta}$$

Here, $\vec{k} = k\hat{z}$ is the beam wave vector, *u(r, z)* is the field radial profile at position z, l is the eigenvalue of the OAM or the so-called topological charge, and θ is the polar angle around the beam propagation axis. The OV beam has a helical

Manuscript received May 26, 2016; revised July 5, 2016; accepted July 11, 2016. Date of publication July 13, 2016; date of current version September 28, 2016. This work was supported by the National Natural Science Foundation of China under Grant 61137001, Grant 91423102, Grant 91323301, Grant 61590930 and Grant 61435005.

Z.-N. Tian, W.-G. Yao, P.-X. Li, Y.-H. Yu, G. Li, and Q.-D. Chen are with the State Key Laboratory on Integrated Optoelectronics, College of Electronic Science and Engineering, Jilin University, Changchun 130012, China (e-mail: chenqd@jlu.edu.cn).

X.-W. Cao is with Department of Mechanical Science and Engineering, Jilin University, Changchun 130025, China.

H.-B. Sun is with the State Key Laboratory on Integrated Optoelectronics, College of Electronic Science and Engineering, Jilin University, Changchun 130012, China, and also with the College of Physics, Jilin University, Changchun 130012, China.

Color versions of one or more of the figures in this letter are available online at http://ieeexplore.ieee.org.

Digital Object Identifier 10.1109/LPT.2016.2591238

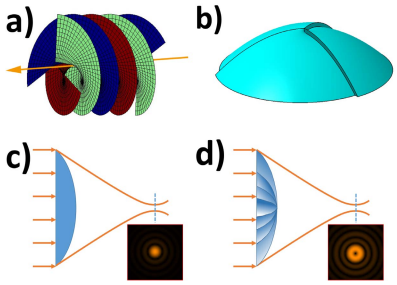

Fig. 1. (a) Helical-phase structure with topological number of three; (b) Schematic diagram of HOVML; (c) ~ (d) the difference of focus situations of focal plane of common microlens and HOVML.

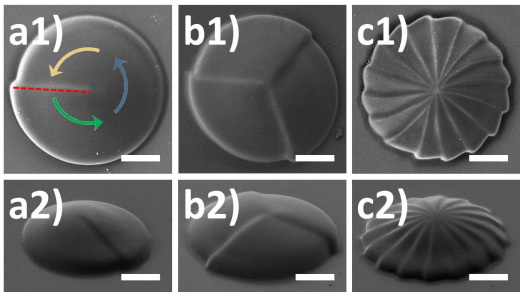

Fig. 2. SEM images of HOVML with topological charge number of (a) 1, (b) 3, (c) 16. (a1) ~ (c1) and (a2) ~ (c2) were taken from top and 60° direction. Scale bar is 10 μm.

phase front, while the shape is decided by the topological charge number, which can take any integer value, positive or negative. Fig. 1(a) shows the helical-phase structure with a topological number of three. The yellow arrow represents the light propagation direction. The phase fronts are helical surfaces, instead of a flat one perpendicular to the propagation direction as a plane wave, which is a significant difference compared to a normal light beam. Here, the novel optical field is generated using the HOVML, whose schematic diagram is shown in Fig. 1(b). For geometric morphology, a spiral phase plate is directly integrated on the surface of a microlens, whose phase delay function can be described as $e^{im\varphi}$. In the schematic diagram, the microlens height is described as *R-sqrt(R^2-r^2)*, where R is the curvature radius of the lens. The spiral phase plate has a suitable curvature designed with the microlens. For the integrated components, a mojarity of the height changes continuously throughout the HOVML, while at positions of $\varphi = 0°$, 120°, and 240°, the height changes are abrupt. They are marked by the red lines in Fig. 1(b). The difference is that the light beams with helical wave fronts focus to rings rather than points. The focus situations of a traditional microlens and the HOVML are illustrated in Figs. 1(c) and 1(d), respectively. If a plane wave passes through the common microlens, a solid light spot could be obtained at the focal plane, as demonstrated in Fig. 1(c). However, a hollow light ring instead of a solid spot is observed on the HOVML, as shown in Fig. 1(d).

The HOVML was fabricated using femtosecond laser-induced two-photon polymerization of commercial negative photoresist SU-8 (2025, MicroChem Corp.). The photoresist has been widely used for the fabrication of high-quality photonic devices and complicated micro-optical elements owing to its high transmittance from the visible to the near-infrared wavelengths, good mechanical properties, and high thermal stability [24], [25]. FsLDW is a technology that has been successfully employed in producing micromechanical and optical microstructures resulting from its unique, high-precision, three-dimensional prototyping capability [26]–[28]. In the experiment, a Ti: sapphire femtosecond oscillator (Tsunami, Spectra Physics) was used as a laser source whose pulse width, wavelength and repetition rate is 120 fs, 780 nm and 80MHz, respectively. The laser beam was tightly focused via an objective lens of NA = 1.4 into the photoresist, whose power was 6 mW measured before the objective lens. The photoresist samples were prepared by spin-coating with a thickness of 20 μm on coverslips which were cleaned by acetone and absolute ethanol. After pre-baking of 3 min at the temperature of 65 °C and 30 min at 95 °C, the focal spot was scanned laterally in the SU-8 film by manipulating a two-galvano-mirror set and along the optical axis by a piezo stage. After scanning, the slide was placed on the hotplate again for 1 min at 65 °C and 10 min at 95 °C for the post-baking. Then the coverslip was immersed in SU-8 developer for 10 min and a solid skeleton was left. Their surfaces were smooth with the roughness less than 10 nm according to an atomic force microscopy measurement [25].

The appearance of the experimentally produced HOVMLs is shown in Fig. 2. The scanning electron microscopic (SEM, JSM-7500F, JEOL) images of the HOVMLs with topological charge numbers of 1, 3, and 16 are demonstrated in Fig. 2, which are obtained at the top and 60° directions. The diameter, height, and focal length of the lenses are 40 μm, 10 μm, and 92 μm, respectively. In contrast to typical microlens, the curved spiral phase plate was directly integrated on the surface of each lens with one-step via FsLDW. The height of curved spiral phase plate with topological charge number of 1 has one abrupt change in the angular direction marked with the read dotted line [Fig. 2(a1), 2(b1)]. The height difference of the two sides is 2.4 μm, considering the refractive index of the environment in the design process. An abrupt phase change of 2π occurs between the two sides of the height change line. While at other locations, the phase and height changes are continuous. From the beginning of the green arrow to the end of the yellow arrow, the phase gradually reduces by 2π [Fig. 2(a1)]. The difference of HOVMLs with topological charge numbers of 3 and 16 is that the abrupt height changes lines are 3 and 16 [Fig. 2(b1), 2(c1)]. The curved spiral phase plate and microlens provide the phase delay in the angle and radius direction, respectively. Finally, with the double-phase modulations, an OV is formed in the rear of the HOVML without converged incident light or additional focus element.

III. Results and Discussion

A significant feature of the HOVML, compared to a normal microlens, is the focusing property of light, which is not limited to a completely coherent laser. When light passes through the HOVML, a hollow light ring is obtained instead of a solid light spot at the focal plane. This unique focusing

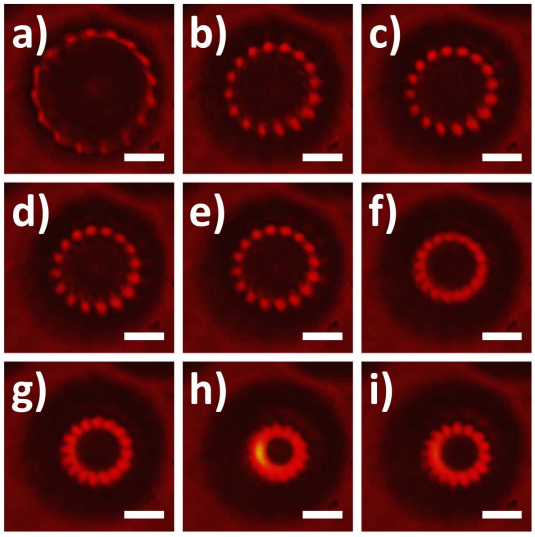

Fig. 3. Experimental energy distribution at different positions behind HOVML. The distance between each picture is 10 μm. (a) $\sim$ (g), (h) and (i) were taken before, on and behind the focal plane, respectively. Scale bar is 10 μm.

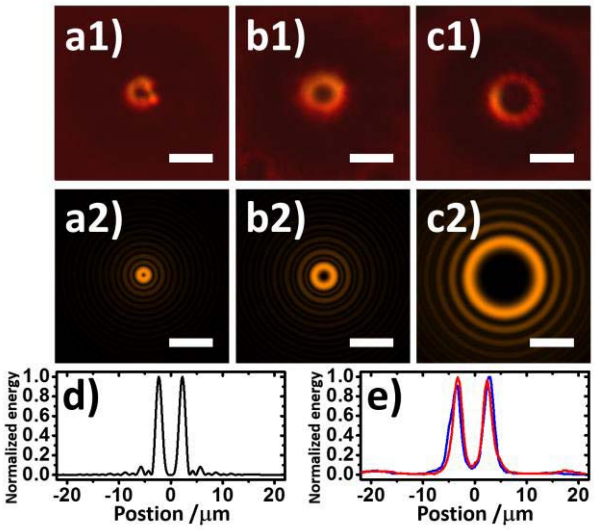

Fig. 4. The focusing properties of HOVML with different topological number. (a1) $\sim$ (c1) Experimental measurement; (a2) $\sim$ (c2) Theoretical simulation result. Scale bar is 10 μm. (d) and (e) Theoretical and experimental normalized energy distribution in the cross section of focal spot.

characteristics were demonstrated using HOVML with the topology charge number of 16, as shown in Fig. 3. The HOVMLs were illustrated using a quasi-monochromatic beam with the wavelength about 600 nm, which was obtained from a collimated sodium lamp with absorption type cutoff filters. At the ear of the HOVML, an objective (60x, OLYMPUS) and a CCD camera (2.2 μm square pixel size, Huaheng Crop.) were fixed on the translational stage as a detection system. By adjusting the position of the objective lens, the focusing results at different positions were detected, as shown in Fig. 3. As can be seen in Figs. 3(a)–3(i), the detector moved away from the HOVMLs, and the distance from the surface of the HOVMLs increased from 22 μm to 102 μm at intervals of 10 μm. The diameter of the hollow light ring decreased gradually until arriving at the focal plane, as can be seen in Fig. 3(h). During the moving process, the dark region in the center of the light spot did not disappear and attained a minimum size on the focal plane. When the detector from the HOVMLs was moved far away, the diameter of the light ring increased [Fig. 3(i)]. On the focal plane, the light spot morphology was a hollow ring instead of a solid point, which is the most intuitive attribute of a vortex light field compared to an ordinary light filed. The optical focusing properties were in accord with the theoretical simulation results, which reflect a high processing accuracy.

The OV carrying an OAM is dissimilar to the spin angular momentum, which has only two values of $\pm\hbar$ (Planck's constant divided by 2π) per photon. A vortex field with a helical phase can carry an intrinsic and eigen OAM of $\pm\ell\hbar$ per photon [1], [2]. In principle, the topological charge ℓ provides unlimited states for the OAM, which makes it possible to carry a large number signals in both classical and quantum communication systems. For different topological charges, the size of the hollow ring on the focal plane is different. The relationship between ℓ and the light size was investigated qualitatively, as demonstrated in Fig. 4. The morphology of the experimental light rings with topological charge numbers of 1, 3, and 16 are demonstrated in Figs. 4(a1)–4(c1). The diameters of the light ring are 4.6 μm, 6.4 μm and 9.3 μm. The morphology light rings with diameters of 2.4 μm, 4.6 μm, and 16.4 μm obtained by simulation are demonstrated in Figs. 4(a2)–4(c2). The regularity of the diameter increase is consistent with the experimental result. The normalized energy distribution of simulation and experiment in the cross section of focal spot are demonstrated in Figs. 4(d) and 4(e), where the focal spot with topological charge number of 3 are used. The red and blue lines in Fig. 4(e) represent the energy distribution in the transverse and longitudinal directions, respectively. The experimental results consist well with the theory.

For more accurate and comprehensive description of the HOVML optical properties, the optical field distribution on the focal plane was simulated using a commercial simulation software, COMSOL Multiphysics (COMSOL Inc.), which was based on the finite element method. An HOVML with a topology number of 16 was utilized in the simulation. The optical field perpendicular to the direction of optical axis was calculated [Fig. 5(a-b)]. The normalized amplitude is a hollow ring with several higher-order diffraction rings [Fig. 5(a)]. However, these higher-order diffraction rings are too weak to be observed in the experiment. The real part of optical field is in the shape of a vortex [Fig. 5(b)]. At the central and the distant position, the real part is zero, representing that the intensity of the light is zero. At other position, along the ring of center point, the real part periodically changes between positive and negative. Light intensity distribution along the optical axis is shown in Fig. 5(c). It was obtained by arranging light intensity distribution over the center at different positions, which ranged from 22 μm to 122 μm on the surface of the lens. Light beam dose not converge into a solid light point at the focal plane marked by red dashed lines.

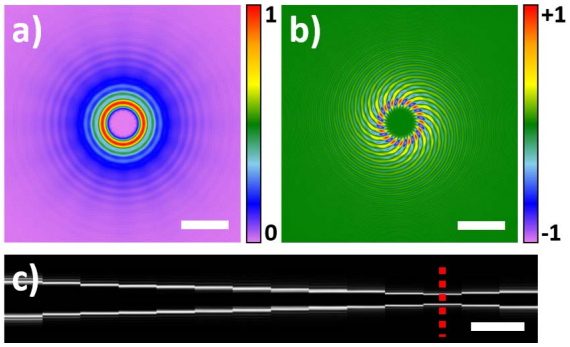

Fig. 5. (a) The normalized amplitude distribution at focal plane; (b) The normalized real part distribution at focal plane; (c) Light intensity distribution along the optical axis. Scale bar is (a) ~ (b) 20 μm, (c) 10 μm.

IV. Conclusions

In summary, we report a novel hybrid refractive–diffractive element, called the HOVML. It consists of a spiral phase plate and a microlens, generating an optical vortex independently without any other optical components. The unique optical properties were demonstrated in the experiment, which is consistent with the theoretical simulation. This HOVML can greatly simplify the OV generation and improve the integration of optical systems. In addition, the novel microlens can be easily integrated on the end facet of optical fiber, which is of significance in optical manipulation and quantum communication. Our findings open up a new avenue to realize highly integrated optical element and offer great convenience to their practical applications.

References

[1] J. Leach, M. J. Padgett, S. M. Barnett, S. Franke-Arnold, and J. Courtial, "Measuring the orbital angular momentum of a single photon," *Phys. Rev. Lett.*, vol. 88, no. 25, p. 257901, Jun. 2002.

[2] L. Allen, M. W. Beijersbergen, R. J. C. Spreeuw, and J. P. Woerdman, "Orbital angular momentum of light and the transformation of Laguerre–Gaussian laser modes," *Phys. Rev. A*, vol. 45, no. 11, pp. 8185–8189, Jun. 1992.

[3] X.-L. Wang, J. Chen, Y. N. Li, J. P. Ding, C.-S. Guo, and H.-T. Wang, "Optical orbital angular momentum from the curl of polarization," *Phys. Rev. Lett.*, vol. 106, no. 18, p. 189301, May 2011.

[4] S. Franke-Arnold, L. Allen, and M. Padgett, "Advances in optical angular momentum," *Laser Photon. Rev.*, vol. 2, no. 4, pp. 299–313, Aug. 2008.

[5] D. G. Grier, "A revolution in optical manipulation," *Nature*, vol. 424, no. 6950, pp. 810–816, Aug. 2003.

[6] Z. J. Yan and N. F. Scherer, "Optical vortex induced rotation of silver nanowires," *J. Phys. Chem. Lett.*, vol. 4, no. 17, pp. 2937–2942, Sep. 2013.

[7] P. Jia, Y. Yang, C. J. Min, H. Fang, and X.-C. Yuan, "Sidelobe-modulated optical vortices for free-space communication," *Opt. Lett.*, vol. 38, no. 4, pp. 588–590, Feb. 2013.

[8] J. Leach *et al.*, "Quantum correlations in optical angle–orbital angular momentum variables," *Science*, vol. 329, no. 5992, pp. 662–665, Aug. 2010.

[9] G. Gibson *et al.*, "Free-space information transfer using light beams carrying orbital angular momentum," *Opt. Exp.*, vol. 12, no. 22, pp. 5448–5456, Nov. 2004.

[10] J. Arlt and K. Dholakia, "Generation of high-order Bessel beams by use of an axicon," *Opt. Commun.*, vol. 177, nos. 1–6, pp. 297–301, Apr. 2000.

[11] J. Kim, Y. M. Li, M. N. Miskiewicz, C. Oh, M. W. Kudenov, and M. J. Escuti, "Fabrication of ideal geometric-phase holograms with arbitrary wavefronts," *Optica*, vol. 2, no. 11, pp. 958–964, Oct. 2015.

[12] A. Schwarz and W. Rudolph, "Dispersion-compensating beam shaper for femtosecond optical vortex beams," *Opt. Lett.*, vol. 33, no. 24, pp. 2970–2972, Dec. 2008.

[13] W. M. Lee, X.-C. Yuan, and W. C. Cheong, "Optical vortex beam shaping by use of highly efficient irregular spiral phase plates for optical micromanipulation," *Opt. Lett.*, vol. 29, no. 15, pp. 1796–1798, Aug. 2004.

[14] E. Brasselet, M. Malinauskas, A. Žukauskas, and S. Juodkazis, "Photopolymerized microscopic vortex beam generators: Precise delivery of optical orbital angular momentum," *Appl. Phys. Lett.*, vol. 97, no. 21, p. 211108, Nov. 2010.

[15] L. Hadžievski, A. Maluckov, A. M. Rubenchik, and S. Turitsyn, "Stable optical vortices in nonlinear multicore fibers," *Light, Sci. Appl.*, vol. 4, p. e314, Aug. 2015.

[16] Y. M. Jung, S. Lee, B. H. Lee, J. Kobelke, and K. Oh, "Observation of tunable bandpass characteristics in a hollow-optical-fiber–microstructured-fiber composite structure using bend-loss edge-shift effects," *Opt. Lett.*, vol. 33, no. 24, pp. 2946–2948, Dec. 2008.

[17] A. V. Smith and D. J. Armstrong, "Generation of vortex beams by an image-rotating optical parametric oscillator," *Opt. Exp.*, vol. 11, no. 8, pp. 868–873, Apr. 2003.

[18] K. T. Gahagan and G. A. Swartzlander, "Optical vortex trapping of particles," *Opt. Lett.*, vol. 21, no. 11, pp. 827–829, Jun. 1996.

[19] T. Lei *et al.*, "Massive individual orbital angular momentum channels for multiplexing enabled by Dammann gratings," *Light, Sci. Appl.*, vol. 4, p. e257, Mar. 2015.

[20] S. Juodkazis, K. Nishimura, and H. Misawa, "In-bulk and surface structuring of sapphire by femtosecond pulses," *Appl. Surf. Sci.*, vol. 253, pp. 6539–6544, May 2007.

[21] Z. Deng *et al.*, "Fabrication of large-area concave microlens array on silicon by femtosecond laser micromachining," *Opt. Lett.*, vol. 40, no. 9, pp. 1928–1931, May 2015.

[22] H. Imamoto *et al.*, "Fabrication and characterization of silicon antireflection structures for infrared rays using a femtosecond laser," *Opt. Lett.*, vol. 36, no. 7, pp. 1176–1178, Apr. 2011.

[23] J. A. Grant-Jacob *et al.*, "Micron-scale copper wires printed using femtosecond laser-induced forward transfer with automated donor replenishment," *Opt. Mater. Exp.*, vol. 3, no. 6, pp. 747–754, Jun. 2013.

[24] J. K. Gansel *et al.*, "Gold helix photonic metamaterial as broadband circular polarizer," *Science*, vol. 325, no. 5947, pp. 1513–1515, Sep. 2009.

[25] D. Wu *et al.*, "100% fill-factor aspheric microlens arrays (AMLA) with sub-20-nm precision," *IEEE Photon. Technol. Lett.*, vol. 21, no. 20, pp. 1535–1537, Oct. 15, 2009.

[26] Y. Liao *et al.*, "Formation of in-volume nanogratings with sub-100-nm periods in glass by femtosecond laser irradiation," *Opt. Lett.*, vol. 40, no. 15, pp. 3623–3626, Aug. 2015.

[27] G. van Freymann *et al.*, "Three-dimensional nanostructures for photonics," *Adv. Funct. Mater.*, vol. 20, no. 7, pp. 1038–1052, Apr. 2010.

[28] Q. Sun, K. Ueno, H. Yu, A. Kubo, Y. Matsuo, and H. Misawa, "Direct imaging of the near field and dynamics of surface plasmon resonance on gold nanostructures using photoemission electron microscopy," *Light, Sci. Appl.*, vol. 2, p. e118, Dec. 2013.